Journal of Sustainability for Energy
https://www.acadlore.com/journals/JSE

Numerical Study of Opto-Electrical Properties of a Mixed Halide Methylammonium Lead Halide ($MAPbBr_{3-n}I_n$; n=0, 1, 2 and 3) Based Perovskite Solar Cell

Kunal Chakraborty, Rajib Saha, Mahua Gupta Choudhury, Samrat Paul*

Advanced Materials Research and Energy Application Laboratory, Department of Energy Engineering, North Eastern Hill University, 793022 Shillong, Meghalaya, India

* Correspondence: Samrat Paul (paulsamrat17@gmail.com)

Received: 10-12-2022 **Revised:** 11-05-2022 **Accepted:** 11-29-2022

Citation: K. Chakraborty, R. Saha, M. G. Choudhury, and S. Paul, "Numerical study of opto-electrical properties of a mixed halide methylammonium lead halide ($MAPbBr_{3-n}I_n$; n=0, 1, 2 and 3) based perovskite solar cell," *J. Sustain. Energy*, vol. 1, no. 1, pp. 27-33, 2022. https://doi.org/10.56578/jse010104.

Abstract: In This research article represents the study of optical, and electrical properties of Methylammonium lead ($MAPbBr_{3-n}I_n$; n=0, 1, 2 and 3) ($CH_3NH_3PbI_3$, $CH_3NH_3PbI_2Br$, $CH_3NH_3PbIBr_2$, and $CH_3NH_3PbBr_3$) based Perovskite solar cell. An FTO/TiO_2/ $MAPbBr_{3-n}I_n$/Spiro-OMeTAD/Al based structure with TiO_2 as electron transport layer and Spiro-OMeTAD hole transport layer has been used for this study. The opto-electrical properties such as resonance time period, indirect and direct band gap have been studied. The results shows that the resonance time period, indirect band gap, and direct band gap for each of the Perovskite layer $CH_3NH_3PbI_3$ is 9.09 µs, 1.4 eV and 2.6 eV, for $CH_3NH_3PbI_2Br$ is 6.25 µs, 1.5 eV and 2.7 eV, for $CH_3NH_3PbIBr_2$ is 6.25 µs, 1.7 eV, and 2.8 eV and for $CH_3NH_3PbBr_3$ is 5.55 µs, 2.1 eV and 2.9 eV respectively.

Keywords: Solar cell; Perovskite; SCAPS-1D; Photovoltaic; Opto-electrical; Simulation

1. Introduction

Organic-inorganic Perovskite based solar cellsconsisted of an organic-inorganic based lead compound having basic structure of AMX_3, where X is an anion which is a halide like Br, I, Cl or F and A & M are cations of different atomic radius [1, 2]. The most common organic-inorganic lead-based Perovskite compound studied for photovoltaic application is Methylammonium Lead Iodide, which has $CH_3NH_3^+$cation and has octahedron of PbI_6 to form the crystal structure [3]. Such hybrid organic-inorganic halide PSC has several advantages like greater light absorptivity, charge carrier mobility, higher exciton diffusion length, lower exciton binding energy and tuneable band gap. As a result, the power conversion efficiency (PCE), of the Perovskitesolar cells (PSCs) is higher compared to other photovoltaic devices. Such hybrid halide compound was first introduced by Kojima et al. [4] with $CH_3NH_3PbI_3$ and $CH_3NH_3PbBr_3$ active material for PV application with a PCE up to 3.8%. Later the group further improved the conversion efficiency by the introduction of Perovskite quantum dots along with TiO_2. Spin coating technique was used for fabrication of the solar cells and could record unto 6.5% [5]. Further, extensive research on $CH_3NH_3PbI_3$ solar cell recorded highest conversion efficiency >20% which is higher than any traditional DSSCs [6, 7]. Pb-based PSC is most suitable for Photovoltaic application because of its Physical, Chemical and Opto-electronic properties making it perfect candidate for PV application. These properties lead to a record PCE of 23.8% [8]. Organometallic halide Perovskites, $MAPbX_3$ (X=Br, I, Cl) has been widely studied as it shows excellent photovoltaic properties. A study on improving the morphology of the $CH_3NH_3PbI_3$ based perovskite layers by adding toluenewas presented by Ashurov et al. under different conditions for obtaining the absorber layers [9]. Wang et al. [10] investigated the structural and photophysical properties of single-crystalline $MAPbBr_3$ based Perovskite using temperature-dependent XRD and various spectroscopy techniques and found that this Perovskite undergoes three phase transitions from cubic i.e., to tetragonal, orthorhombic I, and orthorhombic II, as the temperature decrease from 300 K to 20 K. The PSC consists of three layers that are an electron transport layer (ETL), Perovskite active layer, and hole transport layer (HTL). Both the ETL and HTL has an important influence on device performance. TiO_2 and ZnO are the most common materials used for ETL in

the device architecture. A TiO_2 nanosheets/nanoparticles homogeneous hybrid structure as ETL for application in PSCs under ambient conditions and found that the PSCs based on homogeneous hybrid structure shows a maximum power conversion efficiency higher than that of pure TiO_2 nanosheets [11]. Turaeva and Oksengendler [12] demonstrated the Ising model of segregation of halide ions in hybrid perovskites for obtaining the relationship between the long-range order parameter of segregation and temperature under illumination, by allowing the interaction of iodide ions fluctuations with an electron-hole pair generated by the light source. Luo and his group demonstrated a dopant-free spiro-OMeTAD as HTL to improve the ambient stability of planar PSC and found that the device achieved a power conversion efficiency of 16.92% [13].

Many efforts were put forward in understanding the unique structure, optical and electronic properties of PSCs to achieved excellent photovoltaic performance. Some investigations have been carried out to explore good stability and to improve the power conversion efficiency of the PSCs. Methylammonium lead iodide-bromide [MAPb(I1-xBrx)3 (x=0-0.11)] based Perovskite was used as a model system to study its impact on photovoltaic performance by Zhou and his team. The opto-electrical study of the Perovskite suggested that the carrier lifetime in the Perovskite and the charge extraction at the Perovskite/TiO_2 interface are improved in the mixed halide Perovskite samples [14]. A comparative 1D opto-electrical simulation study of the MAPbI3 based PSC was reported by Haidari [15] using solar cell capacitance simulator (SCAPS), the simulation study reveals that due to high field intensity at larger wavelengths, the broader absorption could lead to a significant improvement to the PSC efficiency. Mohebpour et al. [16] studied the structural and optical properties of $CH_3NH_3PbI_{3-x}Br_x$ (x=1-3) based mixed halide PSC for values by employing density functional theory (DFT), the results suggested that adding halogen bromide to $CH_3NH_3PbI_3$ based Perovskite causes the relocation of energy bands in band structure that leads to increase in the band gap. The enhancement of both optical and electrical characteristics of $MAPbI_3$ based PSC' through the addition of gold/silver nanoparticles were studied using Silvaco TCAD-ATLAS (Electrical Modeling) simulation, the simulation study results reveal that the added nanoparticles have improved the external quantum efficiency of the PSC at certain parts of the spectrum [17]. The study of optical and electronic properties of PSCs using simulation-based analysis suggests for the accomplishment of the device with higher energy conversion efficiency. There were studies on different properties such as optical, structural and electrical properties of a novel class of organic-inorganic metal halide based like Perovskite.

In this present work, we have used a simulation software Solar Cell Capacitance Simulator (SCAPS) 1D to study the optical and electrical properties viz. absorption coefficient, optical band gap, impedance, conductance, resonance time period for the four Perovskite absorbing layer, $CH_3NH_3PbI_3$, $CH_3NH_3PbI_2Br$, $CH_3NH_3PbIBr_2$, and $CH_3NH_3PbBr_3$, respectively. The relevant parameters of SCAPS-1D simulator have been incorporated in the device parameters table section.

2. Simulation Method

For our study we have used SCAPS-1D simulator for study the various optical and electrical properties of the $CH_3NH_3PbI_3$, $CH_3NH_3PbI_2Br$, $CH_3NH_3PbIBr_2$, and $CH_3NH_3PbBr_3$absorbing layer for the FTO/TiO_2/$MAPbBr_{3-n}I_n$/Spiro-OMeTAD/Al device structure [18, 19]. The schematic diagram of device is shown in Figure 1. Here, TiO_2 is electron transport layer (ETL) and Spiro-OMeTAD is hole transport layer (HTL). FTO and Al is used as front contact and back contact electrode respectively. The thickness of the absorbing material is taken as 1.0 µm (optimal) for our study under optimal temperature condition with 1000 W/m^2 solar power AM 1.5 G illumination [20, 21]. The optimum thickness of the absorbing materials is associated with the four factors PCE, V_{OC}, I_{SC}, and FF which are directly measured the device performance. The details of basic parameters for the absorbing layer ($CH_3NH_3PbI_3$, $CH_3NH_3PbI_2Br$, $CH_3NH_3PbIBr_2$, and $CH_3NH_3PbBr_3$), base material (TiO_2, Spiro-OMeTAD, FTO) and metal (Al) have been shown in Table 1 and Table 2 respectively.

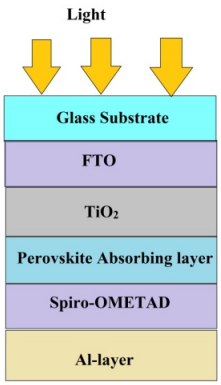

Figure 1. The schematic view of FTO/TiO_2/$MAPbX_3$/Spiro-OMeTAD/Pt device

Table 1. The parameters set for $CH_3NH_3PbX_3$ ($MAPbX_3$) based solar cell

Parameters	$CH_3NH_3PbI_3$	$CH_3NH_3PbI_2Br$	$CH_3NH_3PbIBr_2$	$CH_3NH_3PbBr_3$	References
Band gap(eV)	1.59	1.70	2.03	2.31	[22]
Electron affinity(eV)	3.9	3.6	3.45	3.7	[23, 24]
Dielectric permittivity	10	15	6.5	7.5	[25, 26]
Donor density ($1/cm^3$)	0	$1x10^{10}$	Variable	$1x10^{13}$	[27]
Acceptor density ($1/cm^3$)	2.1×10^{17}	$1x10^{10}$	Variable	$1x10^{13}$	[28]
Electron mobility (cm^2/Vs)	10	15	2	24	[19]
Hole mobility (cm^2/Vs)	10	15	2	24	[19]

Table 2. The base material parameters for the PSC device and work function of metals used in simulation

Parameters	FTO [29]	TiO_2 [30]	Spiro-OMeTAD [31]
Thickness (μm)	0.5	0.03	0.3
Band gap(eV)	3.5	3.2	3
Electron affinity(eV)	4	4.26	2.45
Dielectric permittivity	9	9	3
Donor density ($1/cm^3$)	2×10^{19}	$6x10^{19}$	0
Acceptor density ($1/cm^3$)	0	0	$2x10^{18}$
Electron mobility (cm^2/Vs)	20	4	$2x10^{-4}$
Hole mobility (cm^2/Vs)	10	2	$2x10^{-4}$
Parameters	**FTO [29]**	**TiO_2 [30]**	**Spiro-OMeTAD [31]**
Thickness (μm)	0.5	0.03	0.3
Band gap(eV)	3.5	3.2	3
Electron affinity(eV)	4	4.26	2.45
Dielectric permittivity	9	9	3
Donor density ($1/cm^3$)	2×10^{19}	$6x10^{19}$	0
Acceptor density ($1/cm^3$)	0	0	$2x10^{18}$
Electron mobility (cm^2/Vs)	20	4	$2x10^{-4}$
Hole mobility (cm^2/Vs)	10	2	$2x10^{-4}$

3. Results and Discussion

3.1 Study of Optical Properties of the Absorbing Materials

In this section, optical parameters including optical absorption coefficient (A, cm^{-1}), indirect optical transition ($\sqrt{Ahv}$) and direct optical transition $(Ahv)^2$ in form of Tauc plot of the absorbing layer$MAPbX_3$ ($CH_3NH_3PbI_3$, $CH_3NH_3PbI_2Br$, $CH_3NH_3PbIBr_2$, and $CH_3NH_3PbBr_3$) has been studied at the optimized value of thickness and device temperature [32]. The optical absorption coefficient is defined as how far a light with particular wavelength can penetrate the absorbing material before absorption. A lower absorption coefficient leads to lower absorption of light through the absorbing material. On the other side, material direct and indirect band gap nature can be determined from the direct and indirect transition Tauc plot of the material with the help of optical absorption coefficient. Tauc plot for the absorbing layer can be determine by drawing a linear line in that plot to estimate the indirect band gap of the absorbing materials approximately. The mathematical equation to estimate the optical absorption coefficient is defined as [15]:

$$A = (M + \frac{N}{hv})(\sqrt{hv - E_g}) \tag{1}$$

where, h is the Planck's constant, hv is the photon energy (eV), E_g is the band gap (eV) and M, N are optical absorption parameters. For any Perovskite material usually, M is 10^5 and N is 0.

Here, subgraphs (a), (b) and (c) of Figure 2 show the optical absorption coefficient, indirect and direct optical transition Tauc plot for the absorbing layer respectively. By observing the subgraph (a) of Figure 2, the optical absorption coefficient is fall significantly with the wavelength for all the Perovskite materials. At the 300 nm wavelength the optical absorption coefficient of $CH_3NH_3PbI_3$, $CH_3NH_3PbI_2Br$, $CH_3NH_3PbIBr_2$, and $CH_3NH_3PbBr_3$ material is 1.59×10^5 cm^{-1}, 1.56×10^5 cm^{-1}, 1.45×10^5 cm^{-1}, and 1.35×10^5 cm^{-1} respectively. In further look, At the 500 nm wavelength the optical absorption coefficient of $CH_3NH_3PbI_3$, $CH_3NH_3PbI_2Br$, $CH_3NH_3PbIBr_2$, and $CH_3NH_3PbBr_3$ material is 0.94×10^5 cm^{-1}, 0.88×10^5 cm^{-1}, 0.67×10^5 cm^{-1}, and 0.41×10^5 cm^{-1} respectively. This indicates at 300 nm wavelength the penetration of light in the absorbing material is better. Thus, higher photo energy can be achieved at 300 nm wavelength compared to 500 nm wavelength. Optimal wavelength can be determined through the quantum efficiency determination. The reason behind that fall in the absorption of

the absorbing materials after 300 nm wavelength is enhancement of the reflection. Similarly, subgraphs (b) and (c) of Figure 2 show the indirect optical transition Tauc plot, $\sqrt{ahv}$ vs hv and direct optical transition Tauc plot, $(ahv)^2$ vs hv for the absorbing layer and we have drawn a line (Yellow) in the Tauc plot to estimate the indirect and direct band gap of the material. The $CH_3NH_3PbI_3$, $CH_3NH_3PbI_2Br$, $CH_3NH_3PbIBr_2$, and $CH_3NH_3PbBr_3$ material has indirect band gap of 1.4 eV, 1.5 eV, 1.7eV, and 2.1 eV and direct band gap of 2.6 eV, 2.7 eV, 2.8 eV, and 2.9 eV respectively. The following factors are important when selecting absorption layers- band gap (E_g), electron affinity (E_a), relative permittivity (ε_r), donor density (N_D), acceptor density (N_A), electron mobility (μ_n) and hole mobility (μ_p). Leguy et al. [33] using the relativistic quasi particle self-consistent GW approximation (QSGW), showed that the optical response of $MAPbX_3$ (X = I, Br, Cl) is dominated by the transition between the highest valence band the lowest conduction band, (with minor contributions from the second highest VB and the second lowest CB. The nature of the band gap of the absorbing materials $CH_3NH_3PbI_3$, $CH_3NH_3PbI_2Br$, $CH_3NH_3PbIBr_2$, and $CH_3NH_3PbBr_3$ shows that superior direct band gap nature compared to indirect band gap nature. Such superior direct band gap nature of the material indicates that the absorbing material is suitable for both photovoltaic and LED application.

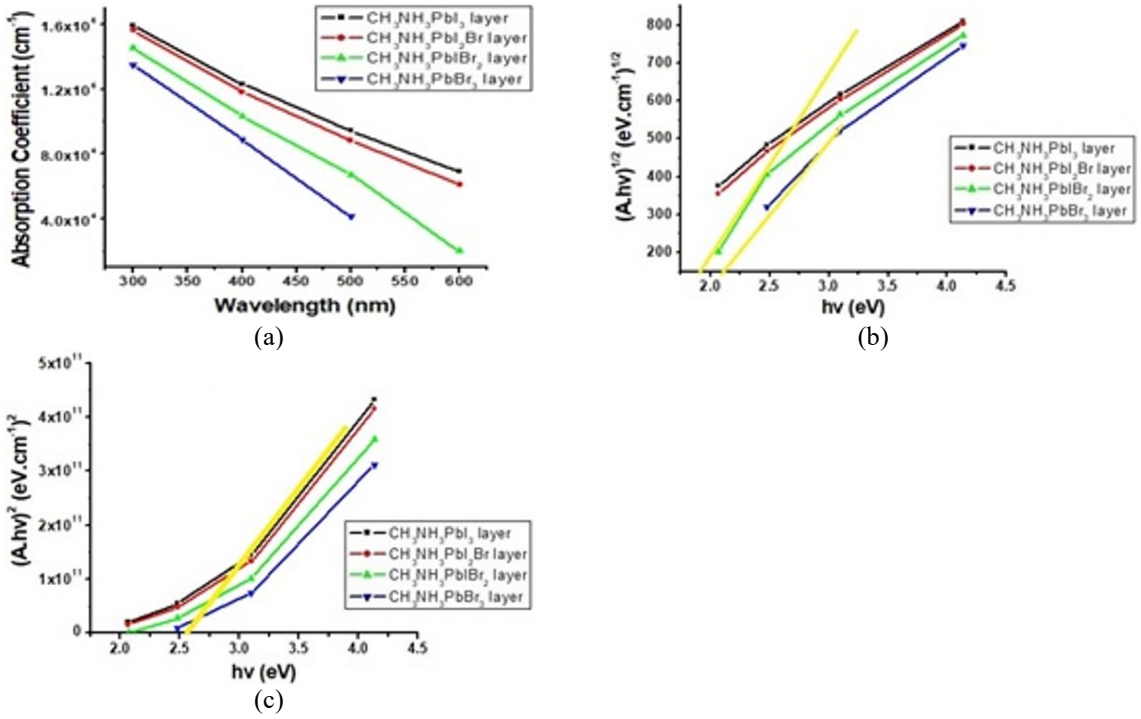

Figure 2. Plot of a) optical absorption coefficient vs wavelength, b) indirect and c) direct optical transition Tauc plot for the $MAPbX_3$ absorbing layer

3.2 Study of Opto-Electrical Properties of the Absorbing Materials

EISA (Electrical Impedance Spectroscopy Analysis) is an effective technique to study the device responses in an AC signal small frequency domain [34]. In EISA, we have used Nyquist plot and Bode plot to find the nature of changes (electronic or ionic) in the device irrespective of response of the device and resonance time period of the device. Two important frequency domain tools Bode plot and Nyquist plot has been studied to find the resonance time period and the nature of changes in the device whether ionic or electronic. Here, subgraphs (a) and (b) of Figure 3 indicate the Bode plot and Nyquist plot of the $MAPbX_3$ solar cell. From the subgraph (a) of Figure 3, it is observed that at 0.11 MHz ($CH_3NH_3PbI_3$), 0.16 MHz ($CH_3NH_3PbI_2Br$), 0.16 MHz ($CH_3NH_3PbIBr_2$) and 0.18 MHz ($CH_3NH_3PbBr_3$) frequency the device has a peak and the corresponding peak time (resonance time) of the material is 9.09 µs ($CH_3NH_3PbI_3$), 6.25 µs ($CH_3NH_3PbI_2Br$), 6.25 µs ($CH_3NH_3PbIBr_2$) and 5.55 µs ($CH_3NH_3PbBr_3$). This faster response of the device indicates all the changes in the device is purely electronic based. By looking at subgraph (b) of Figure 3, it is clearly observed that $CH_3NH_3PbI_3$ absorbing layer has perfect semi-circular Nyquist arc where as for other three absorbing layer $CH_3NH_3PbI_2Br$, $CH_3NH_3PbIBr_2$ and $CH_3NH_3PbBr_3$has inferior semi-circular Nyquist arc shape. Nyquist arc is the parallel formation of shunt resistance (R)-junction capacitance (C) pair in the device. The probable reason behind those dissimilarities in semi-circular shape of Nyquist plot is the existence of multiple reactive elements in the device and as a result a proper parallel RC couple formation is not established in device.

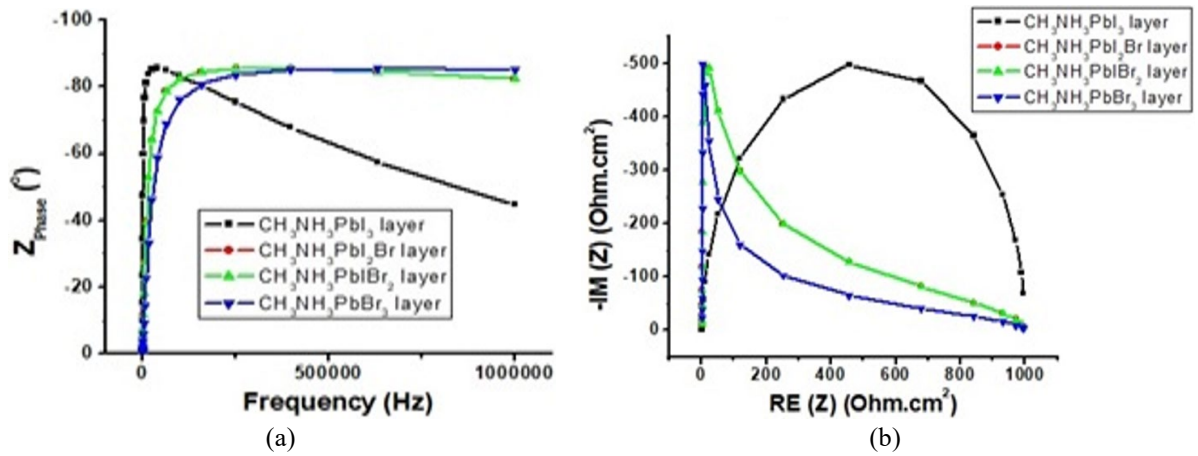

(a) (b)

Figure 3. Impedance analysis: a) Bode plot, b) Nyquist plot for the FTO/TiO_2/$MAPbX_3$/Spiro-OMeTAD/Pt device

The conductivity (G,S/cm^2) of the $CH_3NH_3PbI_2Br$, $CH_3NH_3PbIBr_2$, $CH_3NH_3PbBr_3$, and $CH_3NH_3PbI_3$absorbing material has been studied under the optimal condition. Conductivity of a material is an intrinsic property and it determines the ability to carry the amount of current by that material. Here, Figure 4 shows the G-V graph for the $CH_3NH_3PbI_2Br$, $CH_3NH_3PbIBr_2$, $CH_3NH_3PbBr_3$, and $CH_3NH_3PbI_3$absorbing material. By looking at Figure 4, we can observe that $CH_3NH_3PbI_3$absorbing material has significant enhancement in the conductivity with the open circuit voltage (V) and other three material $CH_3NH_3PbI_2Br$, $CH_3NH_3PbIBr_2$, and $CH_3NH_3PbBr_3$ has no change with the voltage. Optical efficiency is the theoretical basis for $CH_3NH_3PbI_3$ absorption layer to have better current carrying capacity than the other three absorption layers and the external quantum efficiency (EQE), optical absorption coefficient (a) are the useful tool to measure the optical efficiency. This phenomenon suggests that $CH_3NH_3PbI_3$ absorbing layer has superior current carrying capability with compare to other three absorbing layer.

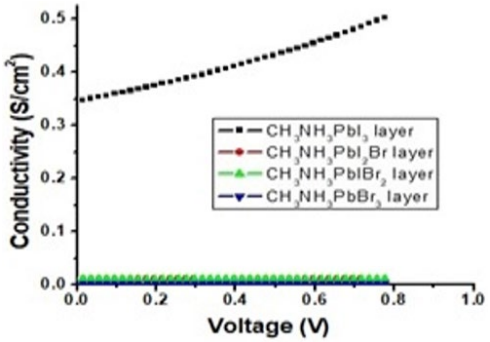

Figure 4. G-V plot for the FTO/TiO_2/$MAPbX_3$/Spiro-OMeTAD/Pt device

4. Conclusions

In this work, optical and electrical properties of mixed halide based Methylammonium lead based PSC has been studied using the SCAPS-1D. Various electrical parameters were investigated to observe its effect on the device performances. The results shows that FTO/TiO_2/$MAPbBr_{3-n}I_n$/Spiro-OMeTAD/Al structure based solar cell device has 9.09 µs, 6.25 µs, 6.25 µs and 5.55 µs resonance time, 1.4 eV, 1.5 eV, 1.7 eV, and 2.1 eV indirect band gap and 2.6 eV, 2.7 eV, 2.8 eV, and 2.9 eV direct band gap respectively for the $CH_3NH_3PbI_2Br$, $CH_3NH_3PbIBr_2$, $CH_3NH_3PbBr_3$, and $CH_3NH_3PbI_3$ absorbing layer, respectively.

Funding

This paper was supported by SERB, DST, New Delhi (Grant No.: EMR/2016/002430 and PDF/2016/002390) for the financial support to carry out this work.

Data Availability

The data used to support the findings of this study are available from the corresponding author upon request.

Acknowledgements

The authors are grateful to the Department of Electronics and Information Systems, University of Gent, Belgium and Prof. Burgelman for providing the SCAPS software to carry out this research work.

Conflicts of Interest

The authors declare no conflict of interest.

References

[1] F. Giustino and H. J. Snaith, "Toward lead-free Perovskite solar cells," *ACS Energy Lett*., vol. 1, no. 6, pp. 1233-1240, 2016. https://doi.org/10.1021/acsenergylett.6b00499.

[2] F. Hao, C. C. Stoumpos, and D. H. Cao, "Lead-free solid-state organic-inorganic halide Perovskite solar cells," *Nat. Photon.*, vol. 8, no. 6, pp. 489-494, 2014. https://doi.org/10.1038/nphoton.2014.82.

[3] N. K. Noel, S. D. Stranks, and A. Abate, "Lead-free organic-inorganic tin halide perovskites for photovoltaic applications," *Energy Environ. Sci*., vol. 7, pp. 3061-3068, 2014. https://doi.org/10.1039/C4EE01076K.

[4] A. Kojima, K. Teshima, Y. Shirai, and T. Miyasaka, "Organometal halide perovskites as visible-light sensitizers for photovoltaic cells," *J. Am. Chem. Soc*., vol. 131, no. 17, pp. 6050-6051, 2009. https://doi.org/10.1021/ja809598r.

[5] E. Jokar, C. H. Chien, and C. M. Tsai, "Robust tin-based Perovskite solar cells with hybrid organic cations to attain efficiency approaching 10%," *J. Adv. Mat.*, vol. 31, no. 2, pp. 1-7, 2019. https://doi.org/10.1002/adma.201804835.

[6] Z. Yi, N. H. Ladi, X. Shai, H. Li, Y. Shen, and M. Wang, "Will organic-inorganic hybrid halide lead perovskites be eliminated from optoelectronic applications," *Nanoscale Adv*., vol. 1, no. 4, pp. 1276-1289, 2019. https://doi.org/10.1039/C8NA00416A.

[7] Q. Wang, Q. Dong, T. Li, A. Gruverman, and J. Huang, "Thin insulating tunneling contacts for efficient and water-resistant Perovskite solar cells," *Adv. Mater.*, vol. 28, no. 31, pp. 6734-6739, 2016. https://doi.org/10.1002/adma.201600969.

[8] C. C. Stoumpos and M. G. Kanatzidis, "Halide perovskites: Poor man's high performance semiconductors," *Adv. Mater.*, vol. 28, no. 28, pp. 5778-5793, 2016. https://doi.org/10.1002/adma.201600265.

[9] N. R. Ashurov, N. S. Ashurov, J. T. Azimov, S. E. Maksimov, and S. S. Rashidova, "Study of possible ways of improving the morphology of layers of the solar radiation absorber in perovskite-based cells," *Appl Sol. Energ*y, vol. 55, no. 1, pp. 8-11, 2019. https://doi.org/10.3103/S0003701X19010031.

[10] K. H. Wang, L. C. Li, M. Shellaiah, and K. W. Sun, "Structural and photophysical properties of methylammonium lead tribromide (MAPbBr3) single crystals," *Sci. Rep*., vol. 7, no. 1, Article ID: 13643, 2017. https://doi.org/10.1038/s41598-017-13571-1.

[11] P. Su, W. Fu, H. Yao, L. Liu, D. Ding, F. Feng, S. Feng, Y. Xue, X. Liu, and H. Yang, "Enhanced photovoltaic properties of Perovskite solar cells by TiO_2 homogeneous hybrid structure," *Roy. Soc. Open Sci*., vol. 4, no. 10, Article ID: 170942, 2017. https://doi.org/10.1098/rsos.170942.

[12] N. N. Turaeva and B. L. Oksengendler, "The Ising Model of the Hoke effect in hybrid perovskites," *Appl Sol. Energy*, vol. 54, no. 4, pp. 318-321, 2018. https://doi.org/10.3103/S0003701X18050195.

[13] W. Luo, C. Wu, D. Wang, Z. Zhang, X. Qi, X. Guo, B. Qu, L. Xiao, and Z. Chen, "Dopant-free Spiro-OMeTAD as hole transporting layer for stable and efficient Perovskite solar cells," *Org. Electron*., vol. 74, pp. 7-12, 2019. https://doi.org/10.1016/j.orgel.2019.06.039.

[14] Y. Zhou, F. Wang, H. H. Fang, M. A. Loi, F. Y. Xie, N. Zhao, and C. P. Wong, "Distribution of bromine in mixed iodide-bromide organo lead perovskites and its impact on photovoltaic performance," *J. Mater. Chem. A*, vol. 4, no. 41, pp. 16191-16197, 2016. https://doi.org/10.1039/C6TA07647E.

[15] G. Haidari, "Comparative 1D optoelectrical simulation of the Perovskite solar cell," *AIP Adv.*, vol. 9, no. 8, Article ID: 085028, 2019. https://doi.org/10.1063/1.5110495.

[16] M. A. Mohebpour, M. S. Hamid, R. Soleimani, and M. B. Tagani, "High performance of mixed halide Perovskite solar cells: Role of halogen atom and plasmonic nanoparticles on the ideal current density of cell," *Physica E Low Dimens. Syst. Nanostruct*., vol. 97, pp. 282-289, 2018. https://doi.org/10.1016/j.physe.2017.11.022.

[17] A. Hajjiah, H. Badran, I. Kandas, and N. Shehata, "Perovskite solar cell with added gold/silver nanoparticles: Enhanced optical and electrical characteristics," *Energies*, vol. 13, no. 15, Article ID: 3854, 2020. https://doi.org/10.3390/en13153854.

[18] K. Chakraborty, M. G. Choudhury, and S. Paul, "Numerical study of Cs_2TiX_6 (X=Br-, I-, F- and Cl-) based Perovskite solar cell using SCAPS-1D device simulation," *J. Sol. Energy*, vol. 194, pp. 886-892, 2019. https://doi.org/10.1016/j.solener.2019.11.005.

[19] F. Sadeghia and M. Neghabi, "Optimization of structure of solar cells based on lead perovskites (CH3NH3PbX3, X: I, Br) via numerical simulation," *J. Sol. Energy Res.*, vol. 2, no. 4, pp. 315-321, 2017.
[20] N. Khoshsirat and N. A. M. Yunus, "Numerical simulation of CIGS thin film solar cells using SCAPS-1D," In 2013 IEEE Conference on Sustainable Utilization and Development in Engineering and Technology, (CSUDET 2013), Malaysia, Selangor, 30 May 2013-01 June 2013, IEEE, pp. 63-67. https://doi.org/10.1109/CSUDET.2013.6670987.
[21] M. Mostefaoui, H. Mazar, and S. Khelifi, "Simulation of high efficiency CIGS solar cells with SCAPS-1D software," *Energy Procedia*, vol. 74, pp. 736-744, 2015. https://doi.org/10.1016/j.egypro.2015.07.809.
[22] T. J. Jacobsson, J. P. Correa-Baena, M. Pazoki, M. Saliba, K. Schenk, M. Grätzel, and A. Hagfeldt, "An exploration of the compositional space for mixed lead halogen Perovskites for high efficiency solar cells," *Energy Environ. Sci.*, vol. 9, no. 5, pp. 1706-1724, 2016. https://doi.org/10.1039/C6EE00030D.
[23] M. Caputo, N. Cefarin, A. Radivo, N. Demitri, L. Gigli, J. R. Plaisier, M. Panighel, G. Di Santo, S. Moretti, A. Giglia, M. Polentarutti, F. De Angelis, E. Mosconi, P. Umari, M. Tormen, and A. Goldoni, "Electronic structure of MAPbI3 and MAPbCl3: Importance of band alignment," *Sci. Rep.*, vol. 9, Article ID: 15159, 2019. https://doi.org/10.1038/s41598-019-50108-0.
[24] J. Huang, S. Xiang, J. Yu, and C. Z. Li, "Highly efficient prismatic Perovskite solar cells," *Energy Environ. Sci.*, vol. 12, no. 3, pp. 929-937, 2019. https://doi.org/10.1039/C8EE02575D.
[25] C. C. Homes, T. Vogt, S. M. Shapiro, S. Wakimoto, and A. P. Ramirez, "Optical response of high-dielectric-constant perovskite-related oxide," *Sci.*, vol. 293, no. 5530, pp. 673-676, 2001. https://doi.org/10.1126/science.1061655.
[26] A. M. Elseman, A. E. Shalan, M. M. Rashad, and A. M. Hassan, "Experimental and simulation study for impact of different halides on the performance of planar Perovskite solar cells," *Mater. Sci. Semicond. Process.*, vol. 66, pp. 176-185, 2017. https://doi.org/10.1016/j.mssp.2017.04.022
[27] N. Kedem, T. M. Brenner, M. Kulbak, N. Schaefer, S. Levcenko, I. Levine, D. Abou-Ras, G. Hodes, and D. Cahen, "Light-induced increase of electron diffusion length in a p-n junction type CH3NH3PbBr3 Perovskite solar cell," *J. Phys. Chem. Lett*., vol. 6, no. 13, pp. 2469-2476, 2015. https://doi.org/10.1021/acs.jpclett.5b00889.
[28] Q. Zhou, D. Jiao, K. Fu, X. Wu, Y. Chen, J. Lu, and S. Yang, "Two-dimensional device modeling of CH3NH3PbI3 based planar heterojunction Perovskite solar cells," *J. Sol. Energy*, vol. 123, pp. 51-56, 2016. https://doi.org/10.1016/j.solener.2015.11.009.
[29] C. Motta, F. El-Mellouhi, and S. Sanvito, "Charge carrier mobility in hybrid halide Perovskites," S*ci. Rep*., vol. 5, no. 1, Article ID: 12746, 2015. https://doi.org/10.1038/srep12746.
[30] S. Z. Haider, H. Anwar, and M. Wang, "Comprehensive device modelling of Perovskite solar cell with inorganic copper iodide as hole transport material," S*emicond. Sci. Technol*., vol. 33, no. 3, Article ID: 035001, 2018. https://doi.org/10.1088/1361-6641/aaa596.
[31] A. Husainat, W. Ali, P. Cofie, J. Attia, and J. Fuller, "Simulation and analysis of methylammonium lead iodide (CH3NH3PbI3) perovskite solar cell with au contact using SCAPS 1D simulator," *Am J. Opt. Photonics*, vol. 7, no. 2, pp. 33-40, 2019. https://doi.org/10.11648/j.ajop.20190702.12.
[32] L. Huang, X. Sun, C. Li, and R. Xu, "Electron transport layer-free planar Perovskite solar cells: Further performance enhancement perspective from device simulation," *Sol. Eng. Mat. Sol. Cells*, vol. 157, pp. 1038-1047, 2016. https://doi.org/10.1016/j.solmat.2016.08.025.
[33] A. M. A. Leguy, P. Azarhoosh, M. Isabel Alonso, M. Campoy-Quiles, O. J. Weber, J. Z. Yao, D. Bryant, M. T. Weller, J. Nelson, A. Walsh, M. van Schilfgaarde, and P. R. F. Barnes, "Experimental and theoretical optical properties of methylammonium lead halide Perovskites," *Nanoscale*, vol. 8, pp. 6317-6327, 2016. https://doi.org/10.1039/C5NR05435D.
[34] L. Contreras-Bernal, S. Ramos-Terrón, A. Riquelme, P. P. Boix, J. Idígoras, I. Mora-Seró, and J. A. Anta, "Impedance analysis of Perovskite solar cells: A case study," *J. Mat. Chem. A*, vol. 7, no. 19, pp. 12191-12200, 2019. https://doi.org/10.1039/C9TA02808K.